Power Engineering and Engineering Thermophysics
https://www.acadlore.com/journals/PEET

Coupled Computational Fluid Dynamics–Aeroacoustic Analysis of Fan Noise: Influence of Rotational Speed, Inflow, and Blade Serrations

Leila Riahinezhad[1], Ahmad Nooraeen[2*], Melika Mohammadkhah[3], Kamran Hassani[4]

[1] Department of Sustainability and Energy, Mammut Group Company, 1513737511 Tehran, Iran
[2] Faculty of Biomedical Engineering, Amirkabir University of Technology, 1149754413 Tehran, Iran
[3] Department of IT and Engineering, IU International University of Applied Sciences-Campus Berlin, 10247 Berlin, Germany
[4] School of Mechanical, Industrial and Aeronautical Engineering, University of the Witwatersrand, 2017 Johannesburg, South Africa

[*] Correspondence: Ahmad Nooraeen (nooraeen@aut.ac.ir; ahmad.nooraeen@gmail.com)

Received: 10-05-2025 **Revised:** 12-30-2025 **Accepted:** 01-07-2026

Citation: L. Riahinezhad, A. Nooraeen, M. Mohammadkhah, and K. Hassani, "Coupled computational fluid dynamics–aeroacoustic analysis of fan noise: Influence of rotational speed, inflow, and blade serrations," *Power Eng. Eng. Thermophys.*, vol. 5, no. 1, pp. 1–17, 2026. https://doi.org/10.56578/peet050101.

Abstract: Reducing aerodynamic noise from rotating fans while preserving their aerodynamic performance remains a major challenge in the design of low-noise flow-control and ventilation systems. Motivated by this challenge, the present study performs a comprehensive numerical investigation of the coupled aerodynamic and aeroacoustic behavior of a rotating fan equipped with straight and serrated trailing-edge blades under both quiescent and inflow operating conditions. The effects of rotational speed, external inflow, and blade trailing-edge geometry on flow structure, pressure distribution, and acoustic response are systematically examined. Simulations are conducted for two rotational speeds and two inlet conditions to isolate rotation-induced mechanisms from inflow-dominated effects governing noise generation and propagation. Aerodynamic results show that under quiescent inflow, the flow field is primarily driven by fan rotation, leading to localized acceleration, non-uniform outlet mass flow, and a strong dependence on rotational speed. The presence of external inflow leads to a more uniform flow field and increased mass flow rates, while reducing the sensitivity to trailing-edge geometry. Moreover, rotational speed emerges as the dominant factor governing both aerodynamic and acoustic responses. Trailing-edge serrations mainly affect low-frequency acoustic behavior at low rotational speeds under quiescent conditions, whereas their influence diminishes at higher speeds and in the presence of inflow. External inflow also raises baseline acoustic levels and modifies the spatial distribution of the acoustic field. Overall, the results highlight the regime-dependent effectiveness of trailing-edge serrations and underscore the importance of accounting for realistic inflow environments in the aerodynamic and aeroacoustic design of low-noise rotating machinery.

Keywords: Aeroacoustics; Rotating fan; Trailing-edge serrations; Acoustic pressure level; Sound amplitude; Flow-acoustic interaction

1 Introduction

The evolution of modern industrial design has increasingly prioritized the mitigation of noise pollution, transitioning from a secondary consideration to a primary engineering constraint [1]. Axial fans, as fundamental components in thermal management, HVAC systems, and propulsion modules, represent a significant source of aeroacoustic emissions [2]. The noise generated by these systems is not merely an environmental nuisance but a marker of aerodynamic inefficiency and structural vibration [3]. It is well-established that the interaction between a rotating blade and the surrounding fluid medium triggers a cascade of pressure fluctuations [4], originating from the turbulent boundary layer and the subsequent wake shedding, that manifest as both broadband noise and discrete tonal components. As rotational speeds increase, the energy contained within these turbulent structures scales exponentially, necessitating a deeper understanding of the near-field flow physics [5]. The complexity of these interactions is further compounded when the fan operates in non-quiescent environments, where external inflow conditions introduce additional layers of turbulence and non-uniformity into the system [6]. The physical

mechanisms underlying fan noise are primarily governed by the unsteady loading of the blades and the thickness of the displacement layer at the trailing edge [7]. The literature often refers to the Lighthill analogy and its subsequent derivations as the foundational framework for understanding how fluid motion is converted into acoustic energy [8]. In the context of axial fans, the dipolar source term, resulting from the fluctuating force exerted by the blade on the fluid, is typically the dominant noise contributor [9]. Previous research has consistently demonstrated that the spatial distribution of these pressure fluctuations is highly concentrated at the blade tips, where the relative velocity is at its maximum [10]. These acoustic hotspots are the primary targets for geometric optimization.

To reduce noise, the modification of the blade's trailing-edge geometry has emerged as one of the most effective passive control strategies [11]. The concept seeks to disrupt the spanwise correlation of the shedding vortices. Traditional straight-edged blades facilitate the formation of large-scale, coherent structures that shed simultaneously across the span, creating a powerful and synchronized acoustic pulse [12]. By introducing serrations, whether sinusoidal, sawtooth, or notched, engineers can force a phase shift in the pressure fluctuations [13]. Scholarly works have provided extensive evidence that these serrations act as a mechanism for vortex breaking, where large eddies are fragmented into smaller, less energetic filaments [14, 15]. This process not only redistributes the acoustic energy across a broader frequency spectrum but also reduces the peak sound amplitude (SA) by promoting destructive interference at the blade edge [16]. The sensitivity of the acoustic field to the specific shape of the serration cannot be overstated. Experimental studies have shown that the depth and wavelength of the serrations must be carefully tuned to the local boundary layer thickness to achieve optimal results [17]. For instance, in low-rotational speed regimes, the impact of the edge geometry might be subtle, as the turbulent energy is insufficient to be significantly affected by the serration scale [18]. However, as the rotational speed increases, the interaction becomes more violent, and the role of the serrated edge in managing the wake-induced noise becomes more pronounced [19].

A critical yet often overlooked aspect of fan aeroacoustics is the influence of the global boundary conditions and the presence of an external inflow velocity. In real-world applications, fans rarely operate in a perfectly still environment; they are subjected to crosswinds, duct constraints, or directed inlet flows that fundamentally alter the flow topology [20, 21]. The introduction of an inlet velocity can change the fan's operation, which is frequently explored through the lens of mass flow distribution and outlet uniformity. Previous investigations into fan-in-duct systems have shown that an imposed inflow velocity acts to homogenize the flow field, reducing the steep pressure gradients typically observed in quiescent tests [22, 23]. This homogenization has a direct impact on the acoustic propagation, as the background flow acts as a medium that can either amplify or mask the noise generated by the blades [24]. Furthermore, the interaction between the incoming flow and the rotating blades introduces a directional bias into the pressure field. While a fan operating in a zero-velocity environment exhibits a largely symmetric pressure distribution relative to its axis [25], the introduction of a velocity vector breaks this symmetry, shifting the pressure peaks and altering the far-field acoustic radiation pattern. Studies using computational fluid dynamics have demonstrated that the velocity streamlines within the domain undergo a significant reorganization when an external flow is present [26]. This change in flow topology suggests that the masking effect of the inlet velocity may reduce the relative impact of blade geometry on the global mass flow [27], as the momentum of the external stream begins to dictate the fluid transport through the domain.

Recent simulations often employ hybrid methods, where the unsteady flow field is solved using Large Eddy Simulation or Detached Eddy Simulation, and the acoustic propagation is calculated via the Ffowcs Williams-Hawkings (FW-H) analogy [28, 29]. These models are particularly adept at capturing the Surface Acoustic Pressure Level (SAPL) on the confining walls of the computational domain, which serves as a proxy for the noise perceived by the surrounding environment [30]. SAPL distribution is highly sensitive to the convective transport of pressure fluctuations [31]; As the fluid advects toward the outlet, it transports acoustic energy, resulting in elevated noise levels concentrated near the downstream boundaries of the domain. Frequency-domain analysis remains the gold standard for interpreting the output of these complex simulations. By extracting the SA at various monitoring points, A clear distinction can be made between the tonal noise associated with the blade-passing frequency and the broadband noise arising from turbulence [32].

This study, therefore, presents a rigorous numerical examination of the aeroacoustic and aerodynamic characteristics of an axial fan, focusing specifically on the impact of trailing-edge serrations under a diverse range of operational conditions such as blade geometries, rotational speed, and various inlet boundary conditions. The study is structured around a comparative analysis of two distinct blade geometries, a standard straight-edged configuration and a specialized serrated-edge design, operating at rotational speeds. The computational domain is constructed to capture both the near-field pressure fluctuations on the blade surfaces and the far-field propagation through a cylindrical volume. In this work, we conduct a series of high-fidelity simulations to extract and analyze a range of key parameters. This multi-faceted approach enables a comprehensive assessment of how geometric modifications interact with rotational and environmental variables to influence the overall performance of the fan system.

2 Materials and Methods

2.1 Geometry and Computational Domain

Figure 1 presents the computational domains, fan configurations, and measurement locations considered in this study. As illustrated in Figure 1a, two axial fans with identical overall dimensions but different trailing-edge geometries are investigated: one fan with a straight trailing edge and another with a serrated trailing edge. This configuration allows the isolated assessment of the effect of trailing-edge shape on aerodynamic noise generation while keeping all other geometric parameters unchanged.

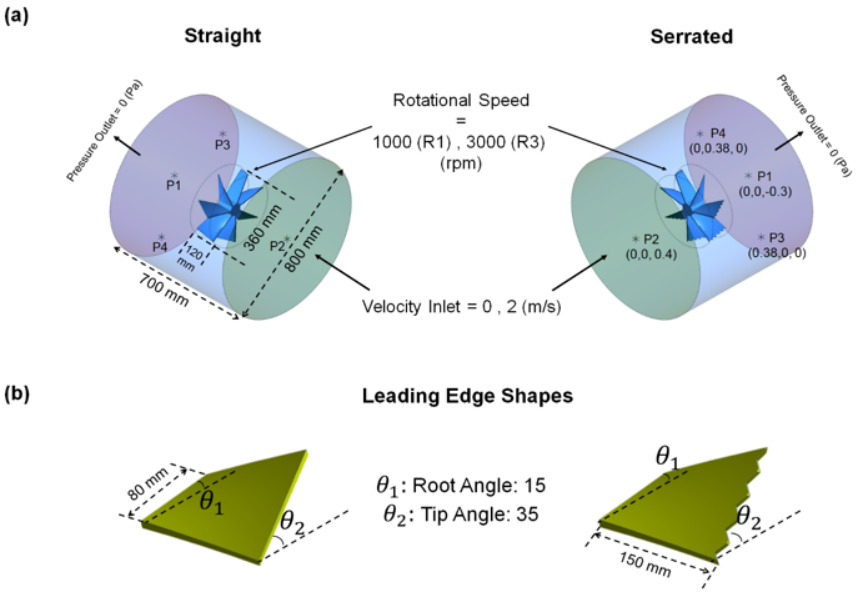

Figure 1. Schematic of the computational domain and boundary conditions

Both fans have an outer diameter of 360 mm and a height of 120 mm and are centrally located within a cylindrical computational domain representing the surrounding air. The domain has a circular cross-section with a diameter of 800 mm and a height of 700 mm, providing adequate spatial extent to reduce confinement effects and to allow the development and propagation of flow structures and acoustic waves generated by the rotating blades. The fan axis coincides with the axis of the cylindrical domain to preserve geometric and flow symmetry.

To evaluate the acoustic response, four monitoring points, labeled P1 through P4, are defined within the external domain for both fan geometries. At these locations, the SA is extracted and used to characterize the spatial distribution of the radiated noise under different operating conditions.

Figure 1b presents detailed information on the fan blade geometry. Each fan comprises blades with a linear twist distribution, defined by a root pitch angle of 15° and a tip pitch angle of 35°. The blade planform has a chord length of 80 mm and a span of 150 mm. The sole geometric distinction between the two fan models is the trailing-edge configuration: one blade has a smooth, straight trailing edge, whereas the other incorporates a serrated trailing edge designed to modify wake dynamics and suppress coherent vortex shedding, thereby influencing the fan's aeroacoustic behavior.

2.2 Computational Fluid Dynamics Simulation and Governing Equations

All numerical simulations are performed using ANSYS Fluent 16.1. The flow is assumed to be three-dimensional, unsteady (transient), and Newtonian, with constant density and viscosity. Heat transfer effects are neglected, and the flow is treated as isothermal. The governing equations for mass and momentum conservation are the unsteady Reynolds-averaged Navier–Stokes equations, expressed as [33]:

The continuity equation is given by:

$$\frac{\partial \rho}{\partial t} + \nabla \cdot (\rho u) = 0 \tag{1}$$

For incompressible flow with constant density:

$$\nabla \cdot (u) = 0 \tag{2}$$

The momentum equation is given by:

$$\frac{\partial(\rho u)}{\partial t} + \nabla \cdot (\rho u \otimes u) = -\nabla p + \nabla \cdot \left[(\mu + \mu_t)\left(\nabla u + \nabla u^T\right)\right] \tag{3}$$

where, u represents the velocity vector; p is the static pressure; μ represents the molecular dynamic viscosity; and μ_t is the turbulent eddy viscosity.

The transient formulation is essential to capture unsteady flow structures, blade-wake interactions, and time-dependent pressure fluctuations, which are critical for accurate aeroacoustic prediction. Turbulence effects are modeled using the $k-\omega$ turbulence model, which is well suited for rotating machinery and near-wall flows due to its robust performance in regions with adverse pressure gradients [34].

The transport equations for the turbulent kinetic energy k and the specific dissipation rate ω are given by:

$$\frac{\partial(\rho k)}{\partial t} + \nabla \cdot (\rho k \vec{u}) = P_k - \beta^* \rho \omega k + \nabla \cdot [(\mu \sigma_k + \mu_t)\nabla k] \tag{4}$$

$$\frac{\partial(\rho \omega)}{\partial t} + \nabla \cdot (\rho \omega \vec{u}) = \alpha \frac{\omega}{k} P_k - \beta \rho \omega^2 + \nabla \cdot [(\mu + \sigma_\omega \mu_t)\nabla \omega] \tag{5}$$

where, P_k is the production of turbulent kinetic energy, and $\alpha, \beta, \beta^*, \sigma_k$, and σ_ω are model constants.

The turbulent eddy viscosity is defined as:

$$\mu_t = \rho \frac{k}{\omega} \tag{6}$$

2.3 Aeroacoustic Modeling

To predict noise generation and propagation, a hybrid aeroacoustic approach is employed. First, the Broadband Noise Source Model available in ANSYS Fluent is used to estimate the local acoustic source strength generated by turbulence–structure interaction, particularly near blade surfaces and wakes. This model is based on semi-empirical formulations derived from Lighthill's acoustic analogy and expresses the acoustic power as a function of turbulence quantities such as turbulent kinetic energy and dissipation rate. This step enables identification of dominant noise-generating regions and provides an initial estimate of broadband noise levels [9].

To compute far-field acoustic pressure fluctuations, the FW-H acoustic analogy is applied in the time domain. The FW-H equation is written as [35]:

$$\frac{1}{c_0^2}\frac{\partial^2 \dot{p}}{\partial t^2} + \nabla^2 \dot{p} = \frac{\partial^2}{\partial x_i x_j}\left[T_{ij} H(f)\right] - \frac{\partial}{\partial x_i}\left[F_i \delta(f)\right] + \frac{\partial}{\partial t}[Q\delta(f)] \tag{7}$$

where, $\dot{p}$, c_0, T_{ij}, $H(f)$, $\delta(f)$, F_i, and Q represent the acoustic pressure fluctuation, speed of sound, Lighthill's stress tensor, Heaviside function, Dirac delta function, dipole and monopole source terms, respectively.

In this study, the FW-H formulation accounts primarily for dipole sources associated with unsteady pressure loading on the blade surfaces, which are dominant in low-Mach-number rotating machinery flows. The FW-H surface is defined around the rotating fan, and time-resolved pressure data from the transient computational fluid dynamics simulation are used as input for acoustic post-processing at the receiver points. Air is used as the working fluid, and its properties are assumed constant throughout the simulations. The values employed in the simulation are summarized in Table 1.

Table 1. Physical properties of air used in the simulations

Constant	Value (Unit)
Density	1.184 (kg/m^3)
Specific heat ratio	1.4
Speed of sound	342 (m/s)
Dynamic viscosity	1.81×10^{-5} (kg/m·s)

2.4 Boundary Conditions

The boundary conditions applied in this study are designed to systematically investigate the effects of fan rotational speed and ambient inflow velocity on the aerodynamic noise generated by different blade geometries. A schematic representation of all imposed boundary conditions is provided in Figure 1. Several operating scenarios are considered by combining two distinct rotational speeds with two inlet flow conditions. The fan rotation is modeled using a rotating reference frame with two prescribed angular velocities: 1000 revolutions per minute (R1) and 3000 revolutions per minute (R3). These values are selected to represent low- and high-speed operating regimes commonly encountered in practical ventilation and cooling applications. For each rotational speed, two inlet velocity conditions are imposed at the outer boundary of the computational domain. In the first case, a zero inlet velocity (V0) is applied, representing a quiescent ambient environment in which the flow is generated solely by the rotating fan. In the second case, a uniform inlet velocity of 2 m/s (V2) is prescribed to model the presence of an external cross-flow or background ventilation. This formulation enables evaluation of the interaction between the incoming flow and the rotating blades, which is known to significantly affect turbulence development, pressure fluctuations, and acoustic emission.

At the outlet boundary of the external domain, a zero gauge-pressure condition is enforced for all simulations. This pressure-outlet specification provides a consistent acoustic reference level and allows pressure waves generated by blade rotation and flow–structure interaction to exit the domain without artificial reflection or constraint. Maintaining identical outlet conditions across all cases ensures direct and meaningful comparisons among different rotational speeds, inlet velocities, and blade geometries.

In total, eight simulation scenarios are systematically designed to examine the individual and combined effects of three key parameters on the aerodynamic and aeroacoustic performance of the fan system. An overview of all cases is provided in Table 2, which summarizes the simulation matrix and facilitates direct comparison across the investigated configurations.

Table 2. Overview of the simulation scenarios, detailing inlet velocities, fan rotational speeds, and trailing-edge geometries

No.	Velocity Inlet (m/s)	Rotational Speeds	Leading Edge Shape
1	0	1000	Straight
2	0	1000	Serrated
3	0	3000	Straight
4	0	3000	Serrated
5	2	1000	Straight
6	2	1000	Serrated
7	2	3000	Straight
8	2	3000	Serrated

The computational domain was discretized using a three-dimensional unstructured mesh to accurately capture the complex flow structures and acoustic source mechanisms around the rotating blades. To ensure the reliability of the numerical results, a mesh independence study was systematically conducted. Several mesh configurations ranging from coarse to progressively finer resolutions were generated and evaluated. For each mesh level, transient simulations were performed and the acoustic power level (APL) was calculated as the primary assessment criterion. The relative difference in APL between two successive mesh refinements was used as the convergence metric. Mesh independence was established once the variation in APL between successive mesh refinements dropped below 2%. Based on this criterion, a mesh with a characteristic element size of 10 mm was selected as an optimal compromise between numerical accuracy and computational efficiency and was therefore adopted for all simulations presented in this study. In addition to spatial discretization, particular attention was given to temporal resolution due to the transient nature of the simulations and the requirement to accurately resolve unsteady flow and acoustic phenomena. A constant time step of 1.0×10^{-4} s was employed for all cases. This time step was chosen to capture the temporal evolution of turbulent structures and pressure fluctuations associated with blade rotation and noise generation, while ensuring numerical stability and maintaining a reasonable computational cost.

2.5 Evaluated Parameters

In the present study, several aerodynamic and aeroacoustic parameters were evaluated in order to provide a comprehensive assessment of the fan performance and noise characteristics under different operating conditions. The APL was analyzed as a key global indicator of noise generation, representing the overall intensity of pressure fluctuations induced by unsteady flow and blade-flow interactions. This parameter provides an integrated measure of the acoustic response and is particularly useful for comparing the noise levels between different rotational speeds, inlet

velocities, and blade geometries. The SAPL was examined to identify the spatial distribution of acoustic sources. SAPL enables the localization of regions with high acoustic activity, which are typically associated with strong turbulence, flow separation, and trailing-edge effects. By comparing SAPL distributions for straight and serrated blade edges, the influence of blade geometry on noise generation mechanisms could be directly assessed. The SA was evaluated at predefined monitoring points in the acoustic field to investigate the frequency-dependent behavior of the emitted sound. Analysis of SA as a function of frequency allows insight into the dominant noise components and their variation with rotational speed and inlet flow conditions, thereby complementing the surface-based acoustic indicators. From an aerodynamic performance perspective, the mass flow rate at the outlet was calculated to quantify the flow capacity of the fan and to evaluate how changes in inlet velocity and blade geometry affect overall throughput. In parallel, the static and total pressure distributions were analyzed to assess the pressure rise generated by the fan and to establish a clear link between aerodynamic loading and acoustic emission. Finally, velocity streamlines were used as a qualitative diagnostic tool to visualize the flow structure within and downstream of the fan. These streamlines provide insight into flow uniformity, vortex formation, and possible separation zones, which are closely related to both aerodynamic efficiency and noise generation. Collectively, these parameter evaluations facilitate a coherent and physically justified interpretation of the fan's coupled aerodynamic and acoustic behavior across all investigated cases.

3 Results

3.1 Acoustic Pressure Level Distribution

As observed in Figure 2, the overall APL levels are consistently higher for the V2 cases compared to the corresponding V0 cases. In addition, for both inlet conditions, increasing the rotational speed from R1 to R3 leads to a pronounced increase in APL, in the R1-V0 case, the maximum APL reaches 98.46 dB, whereas a substantial increase is observed at the higher rotational speed, with the maximum APL attaining 129.1 dB in the R3 cases. When an inlet velocity of V2 is imposed, the peak APL values further increase, reaching a maximum of 133.62 dB. The influence of trailing-edge geometry on the magnitude and distribution of APL is also evident in Figure 2. While the overall maximum APL values are only moderately affected by the blade edge shape, the spatial distribution of APL over the blade surfaces exhibits significant sensitivity to the presence of serrations. In the V2 cases in particular, the serrated blades exhibit lower peak APL values compared to the straight-edged blades, along with a distinctly altered distribution pattern along the trailing edge. For the straight blades, regions of high APL are more concentrated and pronounced, whereas the serrated configuration results in a more dispersed distribution of pressure fluctuations. Across all operating conditions, the minimum APL values are consistently observed near the blade root region. This behavior can be attributed to the lower local relative velocity and reduced aerodynamic loading near the root compared to the mid-span and tip regions, where stronger flow separation and higher turbulence intensity are present.

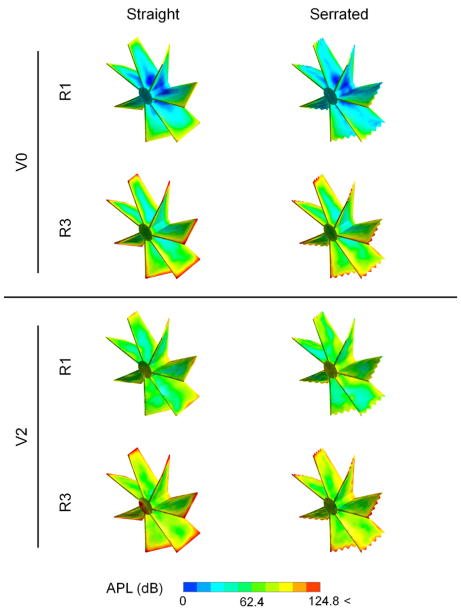

Figure 2. Spatial distribution of acoustic power level (APL) on the fan blade surfaces for rotational speeds of 1000 rpm (R1) and 3000 rpm (R3) under quiescent (V0) and inflow (V2) conditions, comparing straight and serrated trailing-edge blade geometries

3.2 Mass Flow Distribution

The overall mass flow distribution is noticeably more uniform under the V2 inlet condition than under V0. The presence of an imposed inlet velocity promotes a more homogeneous flow field at the outlet, reducing spatial gradients and smoothing the distribution across the outlet surface. In contrast, under the quiescent inlet condition (V0), the mass flow is primarily driven by fan-induced motion, resulting in a more non-uniform pattern (Figure 3). For the V0 cases, a clear dependence of mass flow magnitude on rotational speed is observed. At the lower rotational speed (R1), the mass flow values are significantly smaller than those obtained at R3. Specifically, in the R1-V0 cases, the maximum mass flow reaches approximately 2×10^{-6} kg/s for both straight and serrated trailing-edge configurations, indicating that at this rotational speed the fan induces only a limited throughflow and that the influence of trailing-edge geometry on both the magnitude and spatial pattern of mass flow is negligible. The highest mass flow values are concentrated near the center of the outlet surface, while the lowest values appear near the peripheral regions, reflecting the axial-dominant nature of the induced flow. At the higher rotational speed (R3), the mass flow magnitude increases substantially, with peak values reaching approximately 6×10^{-6} kg/s, which is three times larger than those observed at R1. Moreover, in the R3-V0 cases, the effect of blade trailing-edge geometry becomes more pronounced, leading to noticeable changes in the spatial distribution of mass flow across the outlet surface, even though the global flow direction remains predominantly axial. When an inlet velocity of 2 m/s (V2) is imposed, the mass flow behavior changes significantly. Under these conditions, all cases, regardless of rotational speed or trailing-edge geometry, exhibit similar distribution patterns at the outlet, indicating that the externally imposed inflow dominates the global flow structure. However, the order of magnitude of the mass flow increases dramatically, with peak values reaching approximately 2×10^{-4} kg/s, which is about two orders of magnitude higher than those observed under V0 conditions. Furthermore, in the V2 cases, the influence of blade trailing-edge shape on mass flow becomes negligible. The strong incoming flow overwhelms the subtle geometric effects introduced by the serrations, resulting in nearly identical mass flow distributions for both straight and serrated blades.

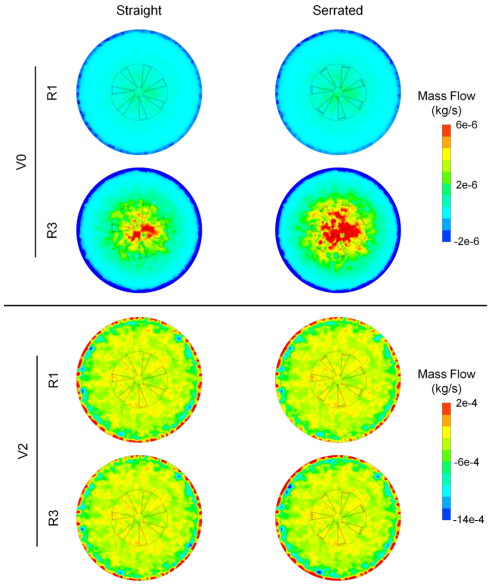

Figure 3. Contours of mass flow distribution at the outlet boundary of the external computational domain for different rotational speeds (R1 and R3), inlet velocity conditions (V0 and V2), and blade trailing-edge configurations

3.3 Pressure Distribution

As shown in Figure 4, the overall pressure range remains comparable between the V0 and V2 cases, spanning approximately from -208 Pa to values exceeding 993 Pa. This indicates that, despite the presence of an external inflow in the V2 cases, the dominant pressure levels within the domain are primarily governed by the rotational motion of the fan rather than by the inlet velocity alone. A clear dependence of the pressure distribution on rotational speed is observed. For both inlet conditions, the R1 cases exhibit a more uniform and smoothly varying pressure field compared to the R3 cases. In particular, under the V0 condition, the maximum pressure in the R1 case reaches approximately 153 Pa, whereas a substantial increase is observed at the higher rotational speed, with the maximum pressure rising to about 982 Pa for the serrated-blade configuration. This pronounced increase highlights the strong influence of rotational speed on pressure loading and local pressure amplification. In all operating conditions, the

highest pressure levels are consistently concentrated near the blade edges for both straight and serrated trailing-edge geometries. However, the serrated blades exhibit higher peak pressure magnitudes in the vicinity of the blade edges compared to the straight blades. This effect is especially pronounced in the R3 cases, where the maximum pressure exceeds 993 Pa. Under the quiescent inlet condition (V0), the pressure distribution around the fan is largely symmetric with respect to the fan axis, reflecting the absence of a preferred flow direction in the far field. Minor asymmetries are observed only in the immediate vicinity of the rotating blades, and the extent of these asymmetries increases with rotational speed, being more noticeable in the R3 cases than in R1. In V2 cases, a similar increase in pressure magnitude and concentration near the blade edges is observed. However, unlike the V0 cases, the far-field pressure distribution loses its axial symmetry. The presence of the incoming flow introduces a directional bias, leading to higher pressure levels near the inlet region compared to the outlet. This results in a distinctly different pressure pattern on the YZ plane, even though the overall pressure range remains comparable to that of the V0 cases.

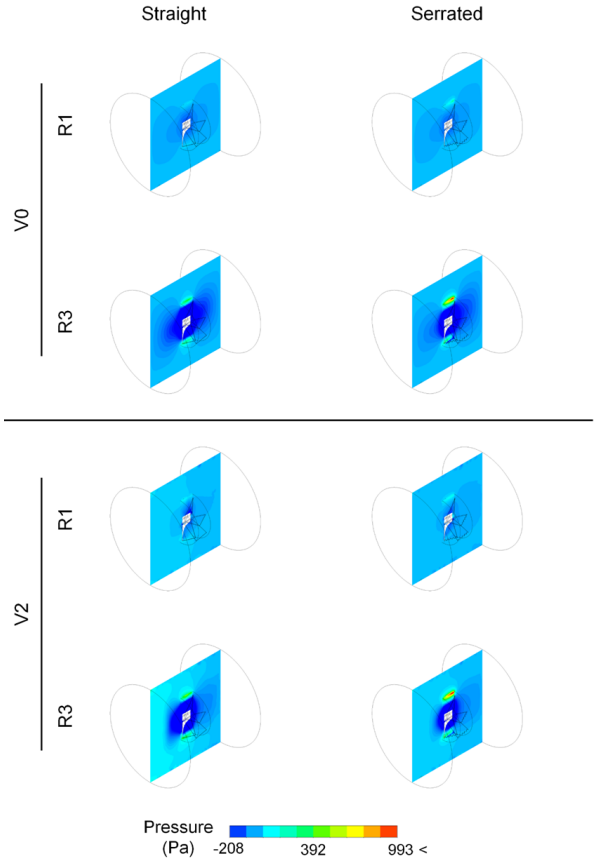

Figure 4. Pressure distribution on the mid-plane (YZ plane) of the computational domain for straight and serrated blades at rotational speeds of 1000 rpm (R1) and 3000 rpm (R3) under both quiescent and inflow conditions

3.4 Surface Acoustic Pressure Level

According to the Figure 5, the overall SAPL levels are consistently higher in the V2 cases than in the corresponding V0 cases. In addition, for both inlet conditions, increasing the rotational speed from R1 to R3 results in higher SAPL values. In the R1-V0 case, the maximum SAPL reaches approximately 17.58 dB and is primarily localized near the upstream and downstream edges of the outer domain. Over most of the wall surface, the SAPL remains within a relatively narrow range of approximately 12.2 to 14.35 dB. Under these conditions, a slight increase in SAPL is observed for the straight trailing-edge configuration, suggesting a modest contribution of the blade edge shape to surface acoustic loading in the absence of an external inflow. At the higher rotational speed (R3), a clear change in both magnitude and spatial distribution of SAPL is observed. In this case, elevated SAPL values are concentrated in the central region of the outer wall, aligned with the axial position of the rotating fan. The influence of blade trailing-edge geometry on SAPL becomes significantly reduced in V2 cases. For both straight and serrated blades, and for both rotational speeds, the magnitude and spatial distribution of SAPL are largely similar. Across all operating conditions, regions of maximum SAPL, exceeding values of 85, are consistently observed near the outlet side of the computational domain.

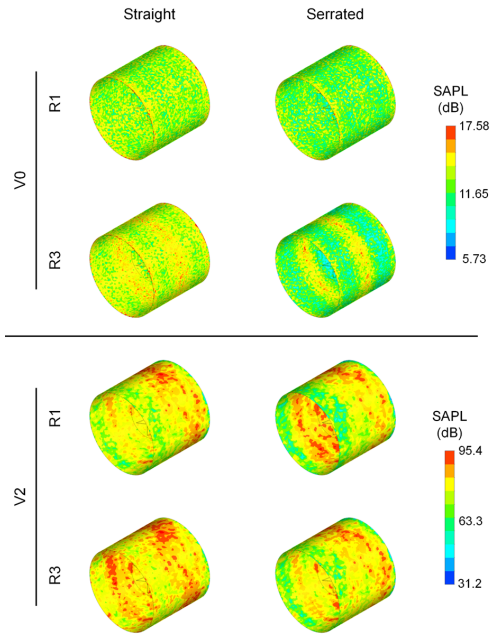

Figure 5. Surface Acoustic Pressure Level (SAPL) distribution on the outer cylindrical wall across various rotational speeds, velocities, and geometries

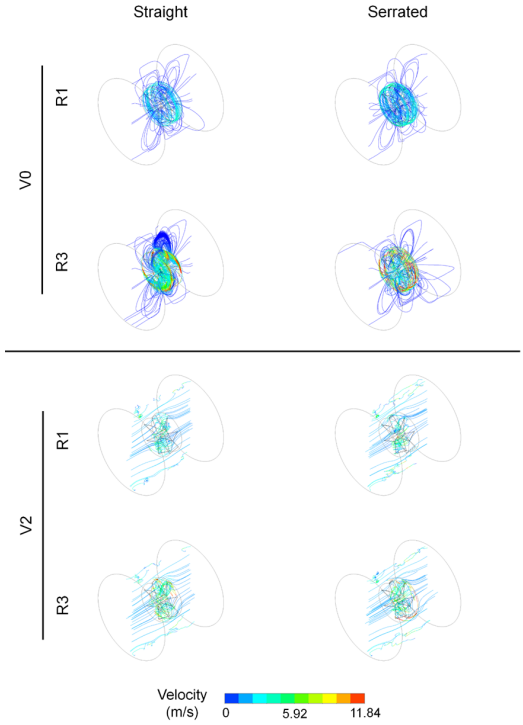

Figure 6. Velocity streamlines and magnitude contours at 1000 and 3000 rpm under quiescent and inflow conditions

3.5 Velocity Streamlines

As shown in Figure 6, the velocity field spans the full range of values in all simulated cases, with the maximum velocity reaching approximately 11.84 m/s. In both inlet conditions, the highest velocities are consistently observed in the vicinity of the fan, particularly near the blade tips, where rotational effects and flow acceleration are strongest. However, while the maximum velocity magnitude remains comparable between cases, the streamline topology differs markedly between the V0 and V2 conditions. Under the quiescent inlet condition (V0), the streamlines are strongly

concentrated around the fan, indicating that the flow field is predominantly governed by the rotational motion of the blades. The induced flow remains largely localized, with pronounced curvature and recirculation patterns in the near-fan region. In contrast, in V2 cases, the streamline pattern changes substantially. The external inflow reduces the localized concentration of streamlines near the fan and enforces a global alignment of the flow with the incoming velocity direction. As a result, streamlines both inside and outside the fan region become more uniformly oriented. A clear dependence of velocity magnitude on rotational speed is also evident. In the R1-V0 case, the maximum velocity reaches approximately 4.83 m/s, whereas in the R3-V0 case the velocity increases significantly, attaining the global maximum value of 11.84 m/s. In contrast, under the V2 condition, all cases, regardless of rotational speed, exhibit local velocity peaks approaching 11.84 m/s at specific locations within the domain. Regarding the effect of blade trailing-edge geometry, the results show that modifications to the trailing-edge shape primarily influence the flow topology rather than the velocity magnitude. While the serrated and straight blades produce distinct streamline patterns, particularly in the near-blade and wake regions, the overall velocity range and peak values remain largely unchanged.

3.6 Sound Amplitude

According to the Figure 7, across all operating conditions, a consistent trend is observed whereby the SA decreases with increasing frequency. At the lower rotational speed (R1), a pronounced influence of trailing-edge geometry on SA magnitude is evident. For the straight trailing-edge configuration, the SA measured at all four monitoring points remains within a range of approximately 0 to 38 dB over the considered frequency band. In contrast, for the serrated trailing-edge configuration at the same rotational speed, the SA levels increase substantially, reaching values of up to approximately 70 dB at low frequencies. This represents nearly a twofold increase in the amplitude range compared to the straight-edge case, indicating that at low rotational speed the serrated geometry enhances low-frequency acoustic radiation under quiescent inflow conditions. In the high-speed cases (R3), this sensitivity to trailing-edge geometry is no longer observed. For both straight and serrated blades, the SA spectra span a similar range, extending from near zero to approximately 87 dB across the frequency domain.

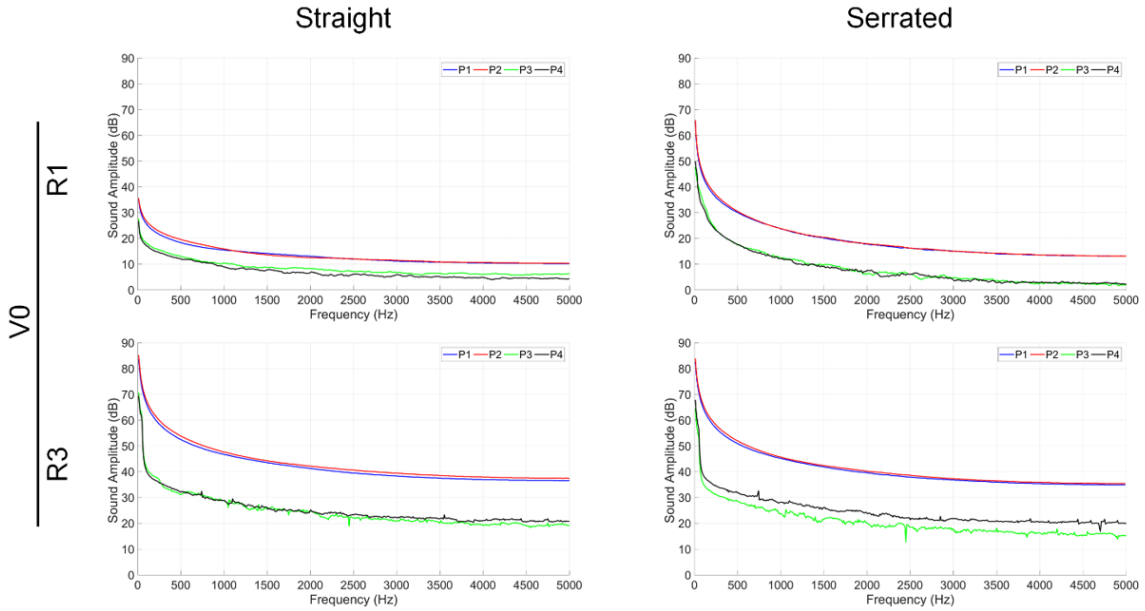

Figure 7. Sound amplitude (SA) spectra at the monitoring points P1–P4 under quiescent inlet conditions (V0) for straight and serrated trailing-edge blades at rotational speeds of 1000 rpm (R1) and 3000 rpm (R3)

Figure 8 presents the SA spectra extracted at the four monitoring points defined in Figure 1 (P1–P4) for the inlet velocity condition V2. In general, the SA spectra under V2 exhibit higher minimum levels compared to the quiescent inflow cases. For the R1 cases, when straight trailing-edge blades are used, the SA values lie within a range of approximately 8 to 42 dB across the frequency domain. In contrast, for the serrated trailing-edge configuration at the same rotational speed, the SA range shifts to approximately 16 to 43 dB. At the higher rotational speed (R3), the maximum SA values for both blade geometries increase to approximately 51 dB, indicating a clear amplification of acoustic emissions with increasing rotational speed. However, a notable reduction in SA is observed at monitoring point P4, where the minimum SA drops to values near 10 dB.

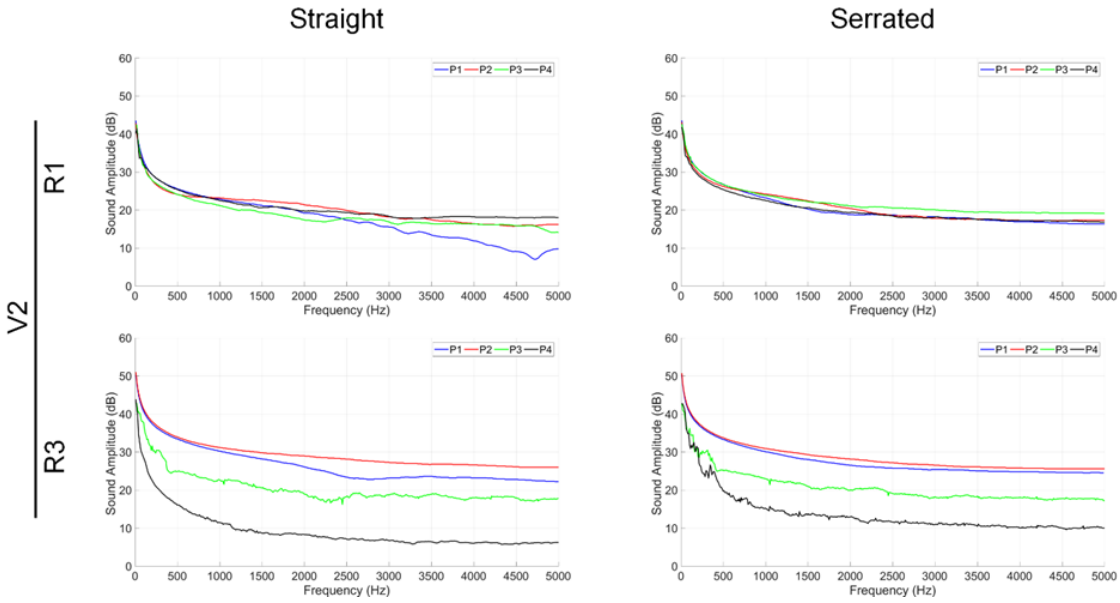

Figure 8. Sound amplitude (SA) spectra at monitoring points P1–P4 for straight and serrated blades at 1000 and 3000 rpm under V2 inflow conditions

4 Discussion

The APL distributions presented in Figure 2 can be interpreted in the broader context of aeroacoustic mechanisms governing rotating blades subjected to both quiescent and externally imposed inflow conditions. The observed increase in APL with rotational speed is consistent with the classical scaling of aerodynamic noise with blade tip speed and turbulence intensity, where higher angular velocities intensify unsteady pressure loading and enhance vortex–blade interactions [36, 37]. Similar trends have been reported in numerical and experimental investigations of axial and centrifugal fans, in which increases in rotational speed led to a disproportionate rise in wall pressure fluctuations and broadband noise levels [38, 39]. The amplification of APL under the V2 inlet condition aligns well with prior works that emphasized the role of inflow turbulence and mean inflow velocity in strengthening unsteady aerodynamic forcing on blade surfaces [40]. External inflow introduces additional large-scale flow structures that interact with the rotating blades, leading to enhanced pressure fluctuation amplitudes, particularly near the leading and trailing edges. Regarding the influence of trailing-edge geometry, the present observation that serrations primarily redistribute APL rather than substantially reducing its maximum value is in line with several computational studies focusing on surface pressure behavior rather than far-field noise [41, 42]. These studies reported that serrations tend to decorrelate pressure fluctuations along the trailing edge, leading to a more spatially diffuse acoustic footprint without necessarily reducing peak surface pressure levels. This mechanism has been attributed to the disruption of coherent vortex shedding and the introduction of spanwise phase variation, which weakens localized pressure concentrations. The more pronounced effect of serrations under the V2 condition further supports the hypothesis that serrated edges interact more effectively with externally imposed turbulent structures than with purely rotation-generated flow, a trend also noted in inflow-turbulence interaction studies [43]. In contrast, some experimental investigations have reported a noticeable reduction in surface pressure fluctuations and associated noise levels due to serrated trailing edges, even at higher rotational speeds [17, 44]. The discrepancy with the present results can be attributed to several factors. First, many of those studies considered optimized serration geometries with larger serration amplitudes or wavelength-to-boundary-layer-thickness ratios specifically tuned for noise reduction, whereas the present configuration may primarily alter flow topology without fully suppressing pressure fluctuation magnitudes. Second, differences in Reynolds number, inflow turbulence characteristics, and measurement focus (far-field sound pressure versus wall-based APL) can lead to divergent conclusions. Serrations are often more effective in reducing radiated noise than in lowering local surface pressure levels, which explains why the present APL-based analysis shows redistribution rather than strong attenuation.

The outlet mass flow distributions in Figure 3 reflect the balance between fan-induced momentum and externally imposed inflow. Under quiescent conditions (V0), the mass flow is controlled mainly by fan rotation, leading to a strong dependence on rotational speed, as widely reported for axial and mixed-flow fans where outlet flow scales with rotational speed in the absence of inflow [45, 46]. The non-uniform patterns observed under V0 are consistent with rotationally induced swirl, hub–tip loading differences, and secondary flows, with higher mass flow concentrated

near the outlet center due to dominant axial momentum [47, 48]. At higher rotational speed (R3-V0), the increased sensitivity to blade geometry agrees with studies showing that stronger blade wakes and higher turbulence levels at elevated tip speeds enhance the influence of local geometric features on outlet flow redistribution [49]. When an inlet velocity is imposed (V2), the flow regime shifts, and the externally driven inflow dominates, resulting in a more uniform outlet mass flow, in line with forced-flow fan studies [50, 51]. Discrepancies with experimental reports of persistent non-uniformity under inflow conditions [52] can be attributed to differences in inlet turbulence, confinement effects, boundary conditions, and the use of an idealized uniform inlet velocity in the present simulations.

Figure 4 indicates that the overall pressure range remains similar under quiescent (V0) and inflow (V2) conditions, implying that pressure generation is primarily governed by rotational effects and blade loading rather than inlet momentum, in agreement with turbomachinery theory and prior numerical studies [46, 48]. At low rotational speed (R1), the smoother and more uniform pressure field is consistent with reduced blade loading and weaker pressure gradients reported for low-speed axial fans. In contrast, the strong pressure amplification observed at R3 aligns with studies showing that higher rotational speed intensifies adverse pressure gradients, flow acceleration near blade edges, and wake–blade interactions [47]. The concentration of peak pressure near the blade edges for both straight and serrated geometries is well documented and attributed to vortex shedding and rapid flow deceleration in trailing-edge regions. The higher local pressures associated with serrated edges, particularly at high rotational speed, agree with findings that serration-induced flow acceleration and small-scale vortical structures enhance near-blade pressure gradients [42]. Finally, the reduced influence of trailing-edge geometry away from the blades supports the consensus that geometric modifications mainly affect near-field pressure and local flow physics, whereas far-field pressure patterns are dominated by global operating parameters such as rotational speed and inlet flow direction [42, 43].

The SAPL distribution on the outer wall reflects the combined effects of blade-generated noise and the convection of pressure fluctuations within the domain. The systematic increase in SAPL under imposed inflow (V2), regardless of rotational speed, is consistent with previous studies showing that mean flow enhances acoustic energy transport and wall loading [53, 54]. At low rotational speed (R1) and quiescent inflow (V0), the low and nearly uniform SAPL levels agree with low-speed fan noise studies, where weak broadband sources dominate and geometric noise-control features have limited impact [55, 56]. In contrast, at higher rotational speed (R3), the localization of elevated SAPL along the axial region of the outer wall aligns with reports linking increased blade loading and tip speed to stronger, axially directed dipole-type acoustic radiation [47, 57]. The diminished influence of trailing-edge geometry under V2 conditions further supports findings that strong inflow and large-scale convective effects dominate the acoustic field at remote boundaries, reducing the effectiveness of localized serration-induced modifications [58].

The streamline patterns in Figure 6 emphasize that the global flow behavior is governed more by flow organization than by peak velocity magnitude, consistent with classical turbomachinery analyses where rotation redistributes momentum while inflow controls large-scale alignment [46]. Under quiescent conditions (V0), the dominance of rotation-induced structures and the confinement of energetic flow near the fan agree with experimental and numerical studies of isolated axial fans, which report strong streamline curvature, recircula1tion, and swirl in the near field [39, 47]. When an inlet velocity is imposed (V2), the marked reorganization of streamlines reflects a transition to a convection-dominated regime. Even moderate inflow suppresses recirculation and enforces a preferred flow direction, as documented in fan–inflow interaction studies [59, 60]. The higher peak velocities at R3 relative to R1 under V0 align with prior measurements [39], whereas the convergence of peak velocities under V2 indicates that the imposed inflow can locally dominate the velocity field, masking rotational-speed effects away from the blades, in agreement with previous study [61]. Finally, the weak sensitivity of velocity magnitude to trailing-edge geometry, despite clear changes in streamline topology, supports previous findings that serrations mainly modify flow coherence, wake structure, and vortex dynamics rather than altering bulk kinetic energy levels [62].

The decay of SA with increasing frequency in Figure 7 reflects the dominance of large-scale, low-frequency noise sources under quiescent inflow, such as blade loading fluctuations and coherent wake structures, which is consistent with established fan-noise theory and prior studies [63, 64]. Reports of flatter spectra in some axial fans can be attributed to higher Reynolds numbers, blade solidity, or tip-clearance effects that enhance broadband turbulence [64], whereas the present configuration preserves coherent low-frequency sources. At low rotational speed, the strong sensitivity of SA to trailing-edge geometry highlights the role of wake coherence. Serrated edges can modify vortex shedding and redistribute acoustic energy; while often associated with broadband noise reduction, they have also been shown to amplify low-frequency sound when interacting with coherent wakes under low-speed, low-turbulence conditions [13, 42, 65]. The absence of external inflow in the present case maintains wake coherence, explaining the observed low-frequency amplification compared to studies with uniform inflow or elevated turbulence levels [42]. At higher rotational speed, the reduced influence of trailing-edge geometry indicates a shift toward turbulence-dominated noise generation, where intense unsteady pressure loading and tip effects overshadow geometric modifications [38, 66]. Although some high-speed studies report continued noise reduction with serrations [67], these typically involve inflow turbulence or ducted environments that weaken coherent structures. The similar spectral trends across monitoring points further indicate a spatially coherent acoustic field governed by

global fan dynamics rather than localized flow features, in agreement with free-field simulations and contrasting with studies involving inflow distortion or confinement [38, 64].

Imposing a uniform inlet velocity elevates the acoustic baseline by introducing persistent aerodynamic fluctuations, consistent with prior numerical and experimental studies on axial and mixed-flow fans where inflow turbulence generates broadband pressure noise even without strong tonal components [38, 68]. At low rotational speed under inflow conditions, trailing-edge geometry remains influential due to active inflow-wake-geometry coupling. Previous works have shown that serrated trailing edges can increase broadband noise by fragmenting coherent inflow structures into multiple distributed pressure sources, particularly under low blade loading [13, 65]. In contrast, noise reductions reported elsewhere are associated with highly turbulent inflow and higher Reynolds numbers, where serrations decorrelate pressure fluctuations rather than scatter them [42]. At higher rotational speed, inflow and rotation jointly cause a redistribution of acoustic energy rather than uniform amplification. Earlier studies demonstrate that mean-flow convection can limit sound-level growth by transporting acoustic disturbances away from receiver locations [53], deviating from the monotonic speed–noise scaling observed under quiescent inflow.

5 Conclusions

This study systematically investigated the coupled aerodynamic and aeroacoustic behavior of a rotating fan equipped with straight and serrated trailing-edge blades under quiescent and inflow conditions, with particular emphasis on the interacting roles of rotational speed, external inflow, and blade geometry. By combining flow-field analysis, surface acoustic pressure evaluation, and frequency-domain SA measurements, the work provides a coherent understanding of how operating and geometric parameters govern both flow organization and acoustic radiation. From an aerodynamic perspective, the results demonstrate that the global flow structure is strongly dictated by the inlet condition. Under quiescent inflow, the flow field is primarily driven by fan-induced motion, leading to localized acceleration, pronounced streamline curvature, and rotational-speed-dependent mass flow redistribution. In contrast, the presence of an imposed inlet velocity enforces a dominant mean-flow direction, homogenizes the outlet mass flow distribution, and reduces sensitivity to blade trailing-edge geometry. These findings confirm that external inflow fundamentally alters the balance between rotation-induced and convection-driven flow mechanisms, particularly at higher rotational speeds.

The acoustic analysis reveals that rotational speed is the primary driver of acoustic intensity, consistently amplifying SAPLs and SA spectra as blade tip speed increases. However, the influence of trailing-edge geometry is shown to be highly conditional. Under quiescent inflow and low rotational speed, serrated trailing edges significantly modify low-frequency SA, indicating an active role of geometry-driven scattering and wake-edge interaction mechanisms. As rotational speed increases, these geometric effects are progressively masked by dominant turbulence generation, blade-tip effects, and strong unsteady pressure loading. The introduction of an external inflow fundamentally reshapes the acoustic response. Inflow conditions elevate the acoustic baseline across monitoring points by introducing persistent aerodynamic fluctuations and enhancing broadband noise content. At the same time, inflow modifies acoustic propagation through convection, redirection, and spatial redistribution of acoustic energy, leading to localized attenuation even at higher rotational speeds. Under these conditions, the influence of trailing-edge serrations becomes secondary and is mainly observable at lower rotational speeds, while at higher speeds the acoustic field is governed by the coupled effects of rotation and mean-flow convection.

Overall, this study highlights that fan aeroacoustic behavior cannot be accurately characterized by rotational speed or blade geometry alone. Instead, it emerges from a complex interaction between flow topology, inflow conditions, and geometric features, with different mechanisms dominating in different operating regimes. The findings underscore the importance of considering realistic inflow conditions when assessing noise-mitigation strategies such as trailing-edge serrations and demonstrate that their effectiveness is strongly regime-dependent. The presented results provide a physically consistent framework for interpreting fan noise behavior and offer valuable guidance for the aerodynamic and acoustic design of low-noise rotating machinery operating under realistic flow environments.

Author Contributions

Conceptualization, L.R. and A.N.; methodology, A.N., M.M, and K.H; software, L.R. and A.N.; validation, A.N., M.M., and K.H.; formal analysis, A.N.; investigation, L.R. and A.N.; resources, L.R. and A.N.; data curation, L.R.; writing—original draft preparation, L.R.; writing—review and editing, M.M. and K.H.; visualization, L.R.; supervision, A.N., M.M., and K.H. All authors have read and agreed to the published version of the manuscript.

Data Availability

The data used to support the research findings are available from the corresponding author upon request.

Conflicts of Interest

The authors declare no conflict of interest.

References

[1] J. Killeen, I. Davis, J. Wang, and G. J. Bennett, "Fan-noise reduction of data centre telecommunications' server racks, with an acoustic metamaterial broadband, low-frequency sound-absorbing liner," *Appl. Acoust.*, vol. 203, p. 109229, 2023. https://doi.org/10.1016/j.apacoust.2023.109229

[2] M. Vourakis, E. Zea, M. Karlsson, N. Andersson, and S. Etemad, "Installation effects on axial fans: Combined aeroacoustic and psychoacoustic perspective," *Appl. Acoust.*, vol. 240, p. 110872, 2025. https://doi.org/10.1016/j.apacoust.2025.110872

[3] M. W. Alhazmi, M. S. Alsoufi, S. A. Bawazeer, H. H. Hijji, H. Alhazmi, and H. F. Alqurashi, "Vibration and aeroacoustic analysis of defective cooling fans: Effects of blade faults on noise, turbulence, and performance efficiency," *J. Umm Al-Qura Univ. Eng. Archit.*, vol. 16, p. 290–305, 2025. https://doi.org/10.1007/s43995-025-00107-2

[4] L. Shang, J. Zhu, X. Huang, S. Gao, Z. Wang, and J. Liu, "Fluid–structure interactions in pump-turbines: A comprehensive review," *Processes*, vol. 13, no. 7, p. 2321, 2025. https://doi.org/10.3390/pr13072321

[5] N. Dangi, J. Sodja, C. S. Ferreira, and W. Yu, "The effect of turbulent coherent structures in atmospheric flow on wind turbine loads," *Renew. Energy*, vol. 241, p. 122248, 2025. https://doi.org/10.1016/j.renene.2024.122248

[6] W. Zhang and M. Vahdati, "A parametric study of the effects of inlet distortion on fan aerodynamic stability," *J. Turbomach.*, vol. 141, no. 1, p. 011011, 2019. https://doi.org/10.1115/1.4041376

[7] D. L. Sutliff, D. L. Tweedt, E. B. Fite, and E. Envia, "Low-speed fan noise reduction with trailing edge blowing," *Int. J. Aeroacoustics*, vol. 1, no. 3, 2002. https://doi.org/10.1260/147547202320962592

[8] W. Layton and A. Novotný, "On lighthill' s acoustic analogy for low Mach number flows," in *New Directions in Mathematical Fluid Mechanics*. Birkhäuser Basel, 2009, pp. 247–249. https://doi.org/10.1007/978-3-0346-0152-8_14

[9] W. Zhao, S. Wasala, and T. Persoons, "Large eddy simulation for aeroacoustic prediction and characterization of electronics cooling axial fans under various operating conditions," *Appl. Acoust.*, vol. 231, p. 110530, 2025. https://doi.org/10.1016/j.apacoust.2025.110530

[10] Z. Yang, C. Cao, J. Fang, B. Zhang, C. Li, and X. Hou, "Mechanism of pressure fluctuations and flow patterns under steady operating conditions of a variable speed pump-turbine," *Processes*, vol. 13, no. 11, p. 1–18, 2025. https://doi.org/10.3390/pr13113511

[11] S. Aleksieienko, A. Dreus, L. Nakashydze, V. Derbaba, and S. Zolotarenko, "Effect of wind turbine blade trailing edge modification on aerodynamic noise," *East.-Eur. J. Enterp. Technol.*, vol. 6, no. 7, p. 53–62, 2025. https://doi.org/10.15587/1729-4061.2025.347020

[12] F. Czwielong, F. Krömer, and S. Becker, "Sound emissions of axial fans with leading-edge serrations on different spanwise locations," in *INTER-NOISE and NOISE-CON Congress and Conference Proceedings, InterNoise19*, Madrid, Spain, 2019, pp. 3993–4998.

[13] B. Lyu, M. Azarpeyvand, and S. Sinayoko, "Prediction of noise from serrated trailing edges," *J. Fluid Mech.*, vol. 793, p. 556–588, 2016. https://doi.org/10.1017/jfm.2016.132

[14] X. Ye, N. Zheng, R. Zhang, and C. Li, "Effect of serrated trailing-edge blades on aerodynamic noise of an axial fan," *J. Mech. Sci. Technol.*, vol. 36, no. 6, p. 2937–2948, 2022. https://doi.org/10.1007/s12206-022-0526-7

[15] W. Zhu and W. Shen, "Airfoil trailing edge noise generation and its surface pressure fluctuation," *J. Power Energy Eng.*, vol. 3, no. 7, p. 14–19, 2015. https://doi.org/10.4236/jpee.2015.37003

[16] A. G. Totu, D. E. Crunțeanu, M. Deaconu, G. Cican, L. Cristea, and C. Leventiu, "Application of passive serration technologies for aero-engine noise control in turbulent inflow environments," *Technologies*, vol. 13, no. 8, p. 1–23, 2025. https://doi.org/10.3390/technologies13080363

[17] C. Arce León, R. Merino-Martínez, D. Ragni, F. Avallone, and M. Snellen, "Boundary layer characterization and acoustic measurements of flow-aligned trailing edge serrations," *Exp. Fluids*, vol. 57, no. 12, p. 1–22, 2016. https://doi.org/10.1007/s00348-016-2272-z

[18] H. Luo, R. Tao, J. Yang, and Z. Wang, "Influence of blade leading-edge shape on rotating-stalled flow characteristics in a centrifugal pump impeller," *Appl. Sci.*, vol. 10, no. 16, 2020. https://doi.org/10.3390/app10165635

[19] K. Ren, S. Zhang, H. Zhang, C. Deng, and H. Sun, "Flow field analysis and noise characteristics of an automotive cooling fan at different speeds," *Front. Energy Res.*, vol. 11, p. 1–13, 2023. https://doi.org/10.3389/fenrg.2023.1259052

[20] J. I. Perén, T. van Hooff, B. C. C. Leite, and B. Blocken, "CFD simulation of wind-driven upward cross ventilation and its enhancement in long buildings: Impact of single-span versus double-span leeward sawtooth roof and opening ratio," *Build. Environ.*, vol. 96, p. 142–156, 2016. https://doi.org/10.1016/j.buildenv.2015.11.021

[21] A. L. Philippou, P. K. Zachos, and D. G. MacManus, "Aerodynamic instabilities in high-speed air intakes and their role in propulsion system integration," *Aerospace*, vol. 11, no. 1, 2024. https://doi.org/10.3390/aerospace11010075

[22] M. Sturm and T. Carolus, "Large scale inflow distortions as a source mechanism for discrete frequency sound from isolated axial fans," in *19th AIAA/CEAS Aeroacoustics Conference*, Berlin, Germany, 2013. https://doi.org/10.2514/6.2013-2105

[23] F. Ahmed, I. Zaman, D. Rezgui, and M. Azarpeyvand, "Aeroacoustics of a ducted fan ingesting an adverse pressure gradient boundary layer," *J. Fluid Mech.*, vol. 985, 2024. https://doi.org/10.1017/jfm.2024.134

[24] C. Yang, R. J. Wallace, and C. Huang, "A review and bibliometric analysis of unmanned aerial system (UAS) noise studies between 2015 and 2024," *Acoustics*, vol. 6, no. 4, p. 997–1020, 2024. https://doi.org/10.3390/acoustics6040055

[25] A. Costantino, M. Musto, G. Rotondo, and A. Zullo, "Numerical analysis for reduced-scale road tunnel model equipped with axial jet fan ventilation system," *Energy Procedia*, vol. 45, p. 1146–1154, 2014. https://doi.org/10.1016/j.egypro.2014.01.120

[26] Y. Zhao, Y. Tian, and Z. Wan, "Aerodynamic characteristics of a ducted fan hovering and transition in ground effect," *Aerospace*, vol. 9, no. 10, p. 572, 2022. https://doi.org/10.3390/aerospace9100572

[27] J. Rendón-Arredondo and S. Moreau, "On the effect of tip flow on the noise of a ducted rotor," *Int. J. Turbomach. Propuls. Power*, vol. 11, no. 1, p. 5, 2026. https://doi.org/10.3390/ijtpp11010005

[28] C. Testa, S. Ianniello, and F. Salvatore, "A Ffowcs Williams and Hawkings formulation for hydroacoustic analysis of propeller sheet cavitation," *J. Sound Vib.*, vol. 413, p. 421–441, 2018. https://doi.org/10.1016/j.jsv.2017.10.004

[29] K. Liu, S. Zhou, X. Li, X. Shu, L. Guo, J. Li, and X. Zhang, "Flow-induced noise simulation using detached eddy simulation and the finite element acoustic analogy method," *Adv. Mech. Eng.*, vol. 8, no. 7, p. 1–8, 2016. https://doi.org/10.1177/1687814016655683

[30] C. Hao, M. Ye, Q. Zhang, Z. Li, X. Zuo, and Z. Sun, "Acoustic-based detection of debonding in thin-layer semi-rigid base asphalt pavements using a-weighted sound pressure levels," *PLoS One*, vol. 20, no. 10, p. 1–26, 2025. https://doi.org/10.1371/journal.pone.0334910

[31] M. Yu, G. Jiang, Y. Jiang, W. Zhang, and J. Sun, "Effect of acoustic waves on the flow and heat transfer around two tandem arranged cylinders," *Case Stud. Therm. Eng.*, vol. 40, p. 102573, 2022. https://doi.org/10.1016/j.csite.2022.102573

[32] N. S. Jamaluddin, A. Celik, K. Baskaran, D. Rezgui, and M. Azarpeyvand, "Experimental analysis of rotor blade noise in edgewise turbulence," *Aerospace*, vol. 10, no. 6, p. 1–18, 2023. https://doi.org/10.3390/aerospace10060502

[33] H. Cai, Z. Zhang, and S. Deng, "Numerical prediction of unsteady aerodynamics of a ducted fan unmanned aerial vehicle in hovering," *Aerospace*, vol. 9, no. 6, p. 318, 2022. https://doi.org/10.3390/aerospace9060318

[34] M. Kirchhofer, M. Krieger, and D. Hofer, "A comparative study on numerical flow simulations of a centrifugal electronic cooling fan using four different turbulence models," *Energies*, vol. 16, no. 23, p. 1–45, 2023. https://doi.org/10.3390/en16237864

[35] Z. Zhou, Y. Liu, H. Wang, and S. Wang, "Mass-conserved solution to the ffowcs-williams and hawkings equation for compact source regions," *Aerospace*, vol. 10, no. 2, p. 1–15, 2023. https://doi.org/10.3390/aerospace10020148

[36] D. Romik and I. Czajka, "Numerical investigation of the sensitivity of the acoustic power level to changes in selected design parameters of an axial fan," *Energies*, vol. 15, no. 4, p. 1357, 2022. https://doi.org/10.3390/en15041357

[37] S. M. Park, S. Y. Ryu, C. Cheong, J. W. Kim, B. Park, Y. C. Ahn, and S. K. Oh, "Optimization of the orifice shape of cooling fan units for high flow rate and low-level noise in outdoor air conditioning units," *Appl. Sci.*, vol. 9, no. 23, p. 1–17, 2019. https://doi.org/10.3390/app9235207

[38] T. Carolus, M. Schneider, and H. Reese, "Axial flow fan broad-band noise and prediction," *J. Sound Vib.*, vol. 300, no. 1–2, p. 50–70, 2007. https://doi.org/10.1016/j.jsv.2006.07.025

[39] J. O. Mo and J. H. Choi, "Numerical investigation of unsteady flow and aerodynamic noise characteristics of an automotive axial cooling fan," *Appl. Sci.*, vol. 10, no. 16, p. 5432, 2020. https://doi.org/10.3390/APP10165432

[40] P. G. Regodeseves and C. S. Morros, "Interaction between flow field and blade forces on HAWT integrating Lagrangian interpolation of velocities with an actuator volume technique," *Renew. Energy*, vol. 256, p. 123766, 2026. https://doi.org/10.1016/j.renene.2025.123766

[41] B. Lyu, M. Azarpeyvand, and S. Sinayoko, "A trailing-edge noise model for serrated edges," in *21st AIAA/CEAS Aeroacoustics Conference*, Dallas, TX, 2016. https://doi.org/10.2514/6.2015-2362

[42] M. Gruber, P. Joseph, and T. Chong, "On the mechanisms of serrated airfoil trailing edge noise reduction," in *17th AIAA/CEAS Aeroacoustics Conference (32nd AIAA Aeroacoustics Conference),*, Portland, Oregon, 2011. https://doi.org/10.2514/6.2011-2781

[43] T. P. Chong and A. Vathylakis, "On the aeroacoustic and flow structures developed on a flat plate with a serrated sawtooth trailing edge," *J. Sound Vib.*, vol. 354, p. 65–90, 2015. https://doi.org/10.1016/j.jsv.2015.05.019

[44] S. Oerlemans, M. Fisher, T. Maeder, and K. Kögler, "Reduction of wind turbine noise using optimized airfoils and trailing-eratdge serions," *AIAA J.*, vol. 47, no. 6, p. 1470–1481, 2009. https://doi.org/10.2514/1.38888

[45] J. F. Gülich, *Centrifugal Pumps*, 3rd ed. Springer, 2007.

[46] S. L. Dixon and C. A. Hall, *Fluid Mechanics and Thermodynamics of Turbomachinery*, 6th ed. Butterworth-Heinemann, 2010.

[47] B. Lakshminarayana, *Fluid Dynamics and Heat Transfer of Turbomachinery*. John Wiley & Sons, 1996.

[48] D. Japikse and N. C. Baines, *Introduction to Turbomachinery*. Concepts ETI/Oxford University Press, 1994.

[49] L. Cao, H. Wang, Y. Ji, Z. Wang, and W. Yuan, "Analysis on the influence of rotational speed to aerodynamic performance of vertical axis wind turbine," *Procedia Eng.*, vol. 31, p. 245–250, 2012. https://doi.org/10.1016/j.proeng.2012.01.1019

[50] S. Becker and T. Heinemann, "Axial fan performance under the influence of a uniform ambient flow field," *Int. J. Rotating Mach.*, vol. 2018, no. 1, p. 6718750, 2018. https://doi.org/10.1155/2018/6718750

[51] S. Castegnaro, "Aerodynamic design of low-speed axial-flow fans: A historical overview," *Designs*, vol. 2, no. 3, p. 1–17, 2018. https://doi.org/10.3390/designs2030020

[52] W. Neise, *Review of Fan Noise Generation Mechanisms and Control Methods*. Publications CETIM, Seulis, France, 1992.

[53] M. E. Goldstein, *Aeroacoustics*. New York: McGraw-Hill, 1976.

[54] X. Zhang, Y. Zhang, and C. Lu, "Flow and noise characteristics of centrifugal fan in low pressure environment," *Processes*, vol. 8, no. 8, p. 985, 2020. https://doi.org/10.3390/PR8080985

[55] M. De Gennaro and H. Kuehnelt, "Broadband noise modelling and prediction for axial fans," in *Proceedings of the International Conference Fan Noise, Technology and Numerical Methods*, Paris, France, 2012.

[56] S. Rama Krishna, A. Rama Krishna, and K. Ramji, "An experimental study on the reduction of motor-fan noise by modification of the blade and shroud configuration," *Proc. Inst. Mech. Eng. Part C J. Mech. Eng. Sci.*, vol. 224, no. 2, p. 315–320, 2010. https://doi.org/10.1243/09544062JMES1869

[57] C. E. Hughes, R. P. Woodward, and G. G. Podboy, "Effect of tip clearance on fan noise and aero dynamic performance," in *11th AIAA/CEAS Aeroacoustics Conference*, Monterey, California, 2005, p. 951–987. https://doi.org/10.2514/6.2005-2875

[58] M. Daroukh, N. Gourdain, S. Moreau, J. F. Boussuge, and C. Sensiau, "Impact of inlet distortion on fan tonal noise," in *12th European Conference on Turbomachinery Fluid dynamics & Thermodynamics*, Stockholm, Sweden, 2017. https://doi.org/10.29008/etc2017-201

[59] B. J. Tester, G. Gabard, and Y. Özyörük, "Influence of mean flow gradients on fan exhaust noise predictions," in *14th AIAA/CEAS Aeroacoustics Conference (29th AIAA Aeroacoustics Conference)*, Vancouver, British Columbia, Canada, 2008. https://doi.org/10.2514/6.2008-2825

[60] Z. Liang, J. Wang, W. Wang, B. Jiang, Y. Ding, and W. Qin, "Numerical and experimental investigations of axial flow fan with bionic forked trailing edge," *Machines*, vol. 11, no. 2, p. 155, 2023. https://doi.org/10.3390/machines11020155

[61] G. Angelini, T. Bonanni, A. Corsini, G. Delibra, L. Tieghi, and D. Volponi, "Effects of fan inflow distortions on heat exchange in air-cooled condensers. unsteady computations with synthetic blade model," in *Proceedings of the ASME Turbo Expo 2018: Turbomachinery Technical Conference and Exposition. Volume 1: Aircraft Engine; Fans and Blowers; Marine*, Oslo, Norway, 2018. https://doi.org/10.1115/GT2018-76518

[62] A. S. Alkhalifa, M. N. Uddin, and M. Atkinson, "Aerodynamic performance analysis of trailing edge serrations on a wells turbine," *Energies*, vol. 15, no. 23, p. 9075, 2022. https://doi.org/10.3390/en15239075

[63] T. F. Brooks, D. S. Pope, and M. A. Marcolini, *Airfoil Self-Noise And Prediction*. NASA Reference Publication, 1989.

[64] M. B. R. Gelot and J. W. Kim, "Effect of serrated trailing edges on aerofoil tonal noise," *J. Fluid Mech.*, vol. 904, 2020. https://doi.org/10.1017/jfm.2020.724

[65] M. S. Howe, "Noise produced by a sawtooth trailing edge," *J. Acoust. Soc. Am.*, vol. 90, no. 1, p. 482–487, 1991. https://doi.org/10.1121/1.401273

[66] M. Gruber, P. F. Joseph, C. Polacsek, and T. P. Chong, "Noise reduction using combined trailing edge and leading edge serrations in a tandem airfoil experiment," in *18th AIAA/CEAS Aeroacoustics Conference (33rd AIAA Aeroacoustics Conference)*, Colorado Springs, CO, 2012. https://doi.org/10.2514/6.2012-2134

[67] T. P. Chong and P. F. Joseph, "An experimental study of airfoil instability tonal noise with trailing edge serrations," *J. Sound Vib.*, vol. 332, no. 24, p. 6335–6358, 2013. https://doi.org/10.1016/j.jsv.2013.06.033

[68] M. V. Lowson, "The sound field for singularities in motion," *Proc. R.*, vol. 286, no. 1407, p. 559–572, 1965. https://doi.org/10.1098/rspa.1965.0164